Title
Impact of vegetation properties on U.S. summer weather prediction

Journal
Journal of Geophysical Research Atmospheres, 101(D3)

ISSN
0148-0227

Authors
Xue, Y
Fennessy, MJ
Sellers, PJ

Publication Date
1996

DOI
10.1029/95JD02169

Peer reviewed

JOURNAL OF GEOPHYSICAL RESEARCH, VOL. 101, NO. D3, PAGES 7419–7430, MARCH 20, 1996

Impact of vegetation properties on U.S. summer weather prediction

Yongkang Xue and Michael J. Fennessy
Center for Ocean-Land-Atmosphere Studies, Calverton, Maryland

Piers J. Sellers
NASA Goddard Space Flight Center, Greenbelt, Maryland

Abstract. Systematic biases in U.S. summer integrations with the Center for Ocean-Land-Atmosphere Studies (COLA) atmospheric general circulation model (GCM) have been identified and analyzed. Positive surface air temperature biases of 2°–4°K occurred over the central United States. The temperature biases were coincident with the agricultural region of the central United States, where negative precipitation biases also occurred. The biases developed in June and became very significant during July and August. The impact of the crop area vegetation and soil properties on the biases was investigated in a series of numerical experiments. The biases were largely caused by the erroneous prescription of crop vegetation phenology in the surface model of the GCM. The prescribed crop soil properties also contributed to the biases. On the basis of these results the crop model has been improved and the systematic errors in the U.S. summer simulations have been reduced. The numerical experiments also revealed that land surface effects on the atmospheric variables at and near the surface during the North American summer are very pronounced and persistent but are largely limited to the area of the anomalous land surface forcing. In this regard, the midlatitude land surface effects described here are similar to those previously found for tropical regions.

1. Introduction

Land surface processes have been shown to have substantial effects on short-term weather predictions and long-term climate projections. Changes in land surface conditions influence the atmospheric circulation by modifying the surface energy balance and hydrological cycle. For example, *Rowell and Blondin* [1990] showed that the 5-day weather forecast for West Africa from the European Center for Medium Range Weather Forecasts (ECMWF) operational forecasting model was sensitive to the surface moisture distribution. *Xue and Shukla* [1993] used the Center for Ocean-Land-Atmosphere (COLA) Studies general circulation model (GCM) to simulate one of the observed African drought anomaly patterns in response to changes in the land surface characteristics. This GCM includes a simplified version of *Sellers et al.*'s [1986] simple biosphere model (SSiB) [*Xue et al.*, 1991].

The simple biosphere model (SiB) [*Sellers et al.*, 1986] was designed to simulate the interactions between the Earth's land surface and the atmosphere by treating the vegetation explicitly and realistically. A comparison between simulations with the COLA GCM coupled to SiB and the same GCM coupled with a conventional hydrological model shows that the coupled biosphere-atmosphere model produces a more realistic partitioning of energy at the land surface [*Sato et al.*, 1989]. Both SiB and SSiB have been validated by using observational data from many field experiments, including the Amazon tropical rainforest experiment [*Sellers et al.*, 1989; *Xue et al.*, 1991], the First ISLSCP International Satellite Land-Surface Climatology Project Field Experiment (FIFE) [*Sellers et al.*, 1992; *Chen et al.*, this issue], the Anglo-Brazilian Amazonian Climate Observation Study [*Xue et al.*, 1995a], the HAPEX-Mobilhy experiment on a crop-grassland site in France [*Shao and Henderson-Sellers*, 1995; *Xue et al.*, 1995b]. These calibrations have provided vegetation and soil property information for some vegetation types, and have led to improvements in the surface biosphere model, resulting in more realistic simulations. However, these field measurements were made at a few sites for only about one third of the SiB vegetation types. Because of differences in spatial scales, the application of data from these site studies to GCM simulations needs further investigation. For vegetation types with little or no observational data, indirect information on vegetation and soil properties from scientific literature has to be used. We will address this problem in more detail in section 2. Although land surface modeling can enhance our ability to understand land surface-atmosphere interactions, poor or inadequate representation of surface processes or land surface conditions may have a negative impact on weather prediction and climate studies.

In this study, systematic errors in U.S. summer seasonal predictions with the COLA GCM have been identified. The simulated June, July, and August (JJA) mean surface temperature in the central U.S. was 2°–4°K higher than observations, and the JJA mean precipitation was about 1 mm d^{-1} (30%) lower than observations in the same region. Similar systematic errors have been noted in other GCMs and weather forecast models. In a 10-year integration using the National Center for Atmospheric Research (NCAR) Community Climate Model (CCM2), *Bonan* [1994] found large systematic warm temperature biases (10°–15°K) in central North America, which A. Hahmann and R. E. Dickinson (personal communication,

Paper number 95JD02169.
0148-0227/96/95JD-02169$05.00

1994) related to the model cloud optical properties. S. Saha and H.-L. Pan (personal communication, 1994) found positive biases of 3°–4°K over the central United States in the near-surface summer temperature forecast by the National Meteorological Center (NMC) operational medium range forecast model. They corrected most of this bias by changing the specification of the SiB minimum stomatal resistance and albedo, which were being used in the land surface parameterization of the model. We will show here that similar systematic errors in the COLA GCM are related to the land surface model.

The model is discussed in section 2. The systematic errors are analyzed in section 3. The surface modeling experiments are presented in sections 4 and 5. The implications from this study are discussed in section 6.

2. Model Description

The COLA GCM is based on a modified version of the National Meteorological Center global spectral model with rhomboidal truncation at zonal wave number 40 [*Sela*, 1980; *Kinter et al.*, 1988; *Fennessy et al.*, 1994]. The prognostic computations are done in the spectral domain, and the physical processes are computed on a grid (approximately 1.8° latitude × 2.8° longitude). The model is discretized into 18 vertical layers. The parameterizations for physical processes include the following:

1. An efficient radiation scheme which resolves the diurnal cycle and includes terrestrial radiative heating [*Harshvardhan et al.*, 1987] and solar radiative heating [*Lacis and Hansen*, 1974; modified by *Davies*, 1982]. An interactive cloud scheme, which is similar to the one developed by *Slingo* [1987], was incorporated into the GCM for the radiation calculations [*Hou*, 1990].
2. The level 2.0 second-order turbulence closure scheme of *Mellor and Yamada* [1982] for subgrid-scale exchanges of heat, momentum, and moisture.
3. A modified Kuo scheme for convection [*Anthes*, 1977; *Kuo*, 1965], shallow convection [*Tiedke*, 1984], and large-scale condensation.
4. A gravity-wave drag parameterization which follows that of *Alpert et al.* [1988].

The SSiB model [*Xue et al.*, 1991], which is a simplified version of the simple biosphere model (SiB) of *Sellers et al.* [1986], is used to model the land surface in the COLA GCM. SSiB has three soil layers and one canopy layer, and eight prognostic variables: soil wetness in three soil layers; temperature at the canopy, ground surface and deep soil layers; water stored on the canopy; and snow stored on the ground.

The force restore method is used to predict the time variation of the soil temperatures. In the three-layer soil model, water movement is described by a finite difference approximation to the diffusion equations. The governing equations for the interception water stores are based on water conservation equations.

There are 12 vegetation types in SiB and SSiB. These include tall vegetation, short vegetation, arable crops, and desert as listed in the work by *Dorman and Sellers* [1989]. The main sources of data for the distribution of the world vegetation types were the physiognomic classification of *Kuchler* [1983] and the land use database of *Matthews* [1984, 1985]. The Matthews data were used to determine areas that were at least 50% cultivated, for which the crop vegetation type (type 12) was assigned. *Kuchler*'s [1983] classification assigned 32 natural vegetation types to land surface areas. These 32 surface types were grouped into the remaining 11 SiB vegetation types.

We found that there are a number of places where Kuchler's classifications differ from the current land surface conditions. Recently, the U.S. Geological Survey (USGS) EROS Data Center and the University of Nebraska-Lincoln have developed a U.S. prototype for a global land cover characteristics database derived from 1-km advanced very high resolution radiometer (AVHRR) satellite data [*Loveland et al.*, 1991]. The Loveland et al. map is significantly different from the Kuchler-Matthews map over the east coast and the Great Plains. One hundred fifty-nine seasonally distinct spectral/temporal land cover classes were labeled according to their constituent vegetation types and productivity [*Loveland et al.*, 1991]. The 159 detailed classes were generalized into the 12 major SiB biomes using an interpretation of each classes vegetation constituents, phenology, elevation, and climatic characteristics [*Reed et al.*, 1994; *Steyaert et al.*, 1994]. This new vegetation map has been introduced into the COLA GCM to prescribe the vegetation types over the United States [*Fennessy and Xue*, 1995].

A parameter set for each of the 12 SiB types was created based on a variety of sources. Some parameters were derived from the calibrations of field measurements as discussed in the Introduction. Many parameters were derived from the biometric and physiological data for representative species in each biome determined from a wide-ranging survey of the ecological and geographical literature [*Dorman and Sellers*, 1989; *Willmott and Klink*, 1986]. Many of the parameters in SiB are invariant with season. However, seasonally varying monthly values of leaf area index and green leaf fraction are prescribed. *Klink and Wilmott* [1985] compiled charts of leaf area index and green leaf fraction annual cycles for each Kuchler vegetation type. The seasonality of the SiB leaf area index and green leaf fraction are based on these charts. The prescription of the crop vegetation type is different: the vegetation cover, leaf area index, greenleaf fraction, leaf orientation, and root length are varied according to the growing season, which is a function of latitude and time.

In the COLA GCM the SSiB parameters are assigned to each grid square based on the input vegetation map and month. These parameters and the solar zenith angle and snow cover determine the surface albedo, and the surface radiation budget. The surface model provides the GCM with the land-atmosphere fluxes of latent heat, sensible heat, momentum, and radiation.

3. Systematic Errors in U.S. Summer Simulations

A large number of boreal summer integrations were conducted using the COLA GCM with different atmospheric initial conditions (1,2,3, June of different years), and different sea surface temperature (SST) boundary conditions for prediction studies. We found that positive surface temperature errors over central North America occurred in each of 30 seasonal integrations examined. Figure 1a shows the difference between the surface effective radiative temperature (30 case mean) and the observed surface air temperature. The global surface air temperature was not saved in these integrations. The effective radiative temperature is some combination of the surface soil temperature and temperature of the vegetation canopy. During summer this temperature is generally higher than the sur-

face air temperature; thus the positive temperature biases shown in Figure 1 tend to be exaggerated. The JJA mean observations were calculated from the National Meteorological Center (NMC), Climate Analysis Center (CAC), Climate Anomaly Monitoring System station data archive (CAMS) [*Ropelewski et al.*, 1985]. The surface temperature errors include a correction for the difference in elevation between the model grid boxes and the observing stations, which tend to be situated in valleys and are generally at a lower elevation than the mean elevation over a GCM grid box. A lapse rate of 6.5°C km^{-1} was used for this correction.

In the eastern United States, the simulated JJA mean temperature was about 4°K higher than the observations with a maximum error of more than 6°K (Figure 1a). This systematic error developed during June and was fully established during July and August (Figures 1b, 1c, and 1d). The maximum errors in July and August were more than 8°K. The JJA mean precipitation in this region was 0.5–1 (10–20%) mm d^{-1} less than that observed (Figure 1e). The surface temperature in the model was calculated using the force restore method and depends on the surface vegetation and soil properties, which depend on the vegetation type in the model. A vegetation map is used in the COLA GCM to assign one vegetation type to each model Gaussian grid box, in which the physical calculations are done (Figure 2a). It is clear that the area with a large positive temperature bias in the central United States is closely associated with the area of vegetation type 12 (Figures 1a and 2a), which is a mixture of crops and deciduous trees. The coincidence of two areas led to the hypothesis that the systematic error may be related to the specification of vegetation type 12 in the surface model.

Experiments have been designed to examine this hypothesis and to understand the causes of the bias. In these experiments, the COLA GCM with the *Loveland et al.* [1995] U.S. vegetation map (Figure 2b) [*Fennessy and Xue*, 1995] was used. The crop area in the United States was reduced in the new map. In particular, most of the crop area in the eastern United States in the old map (Figure 2a, type 12), was replaced by the broadleaf deciduous trees in the new map (Figure 2b, type 2).

A number of numerical experiments have been conducted to test the impact of the new vegetation map on boreal summer simulations [*Fennessy and Xue*, 1995]. Three JJA seasonal integrations with different atmospheric initial conditions and SST boundary conditions were done using the new vegetation map (cases C1, C2, and C3 in Table 1, ensemble referred to as ensemble C).

The JJA surface air temperature systematic errors in ensemble C (Figure 3a) are similar to the equivalent radiative temperature systematic error from the 30 case ensemble (Figure 1a). The magnitude of the surface air temperature error is lower because the effective radiative temperature is usually higher than the surface air temperature in summer. The simulated surface air temperature is shown in Figure 3 and all subsequent figures. The area with positive temperature biases is also reduced in ensemble C, consistent with the smaller extent of the crop area (type 12) in the new vegetation map. The errors in each of the cases C1, C2, and C3 are very similar to the mean error, with the larger errors occurring in July and August (not shown). During these 2 months the maximum errors were more than 6°K. The smaller positive temperature bias over the western coast of the United States will not be addressed here. The systematic bias in the central United States not only occurred at the surface but also in the lower

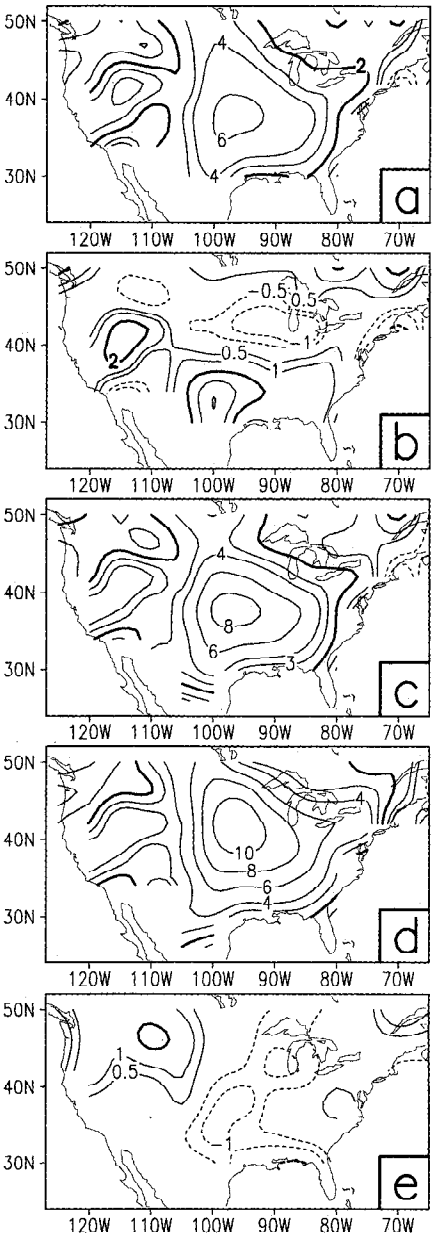

Figure 1. General circulation model (GCM) systematic error (old 30 member ensemble) in (a) June, July, and August (JJA) surface temperature, (b) June surface temperature, (c) July surface temperature, (d) August surface temperature, contours are ±0.5°, 1°, 2°, 3°, 4°, 6°, 8°, 10°C, and (e) JJA precipitation, contours are ± 0.5, 1, 2 mm d^{-1}. Dashed contours are negative.

atmosphere. Figure 4 shows the ensemble C errors relative to the mean of the corresponding analyses of the observations from the European Center for Medium-Range Weather Forecasts (ECMWF). The JJA mean warm temperature bias at 850 mbar was 2°–3°K and was of greater zonal extent than the corresponding surface errors (Figure 4a). The temperature bias at 700 mbar was smaller in magnitude (1°–2°K) and extent (Figure 4b). At 850 mbar the JJA mean specific humidity was about 2 g kg^{-1} (15%) less than the observed (Figure 4c). At 700 mbar there was no apparent systematic specific humidity error (not shown). The wind flow at 850 mbar from the Gulf of Mexico was stronger than observed (Figure 4d). Despite the

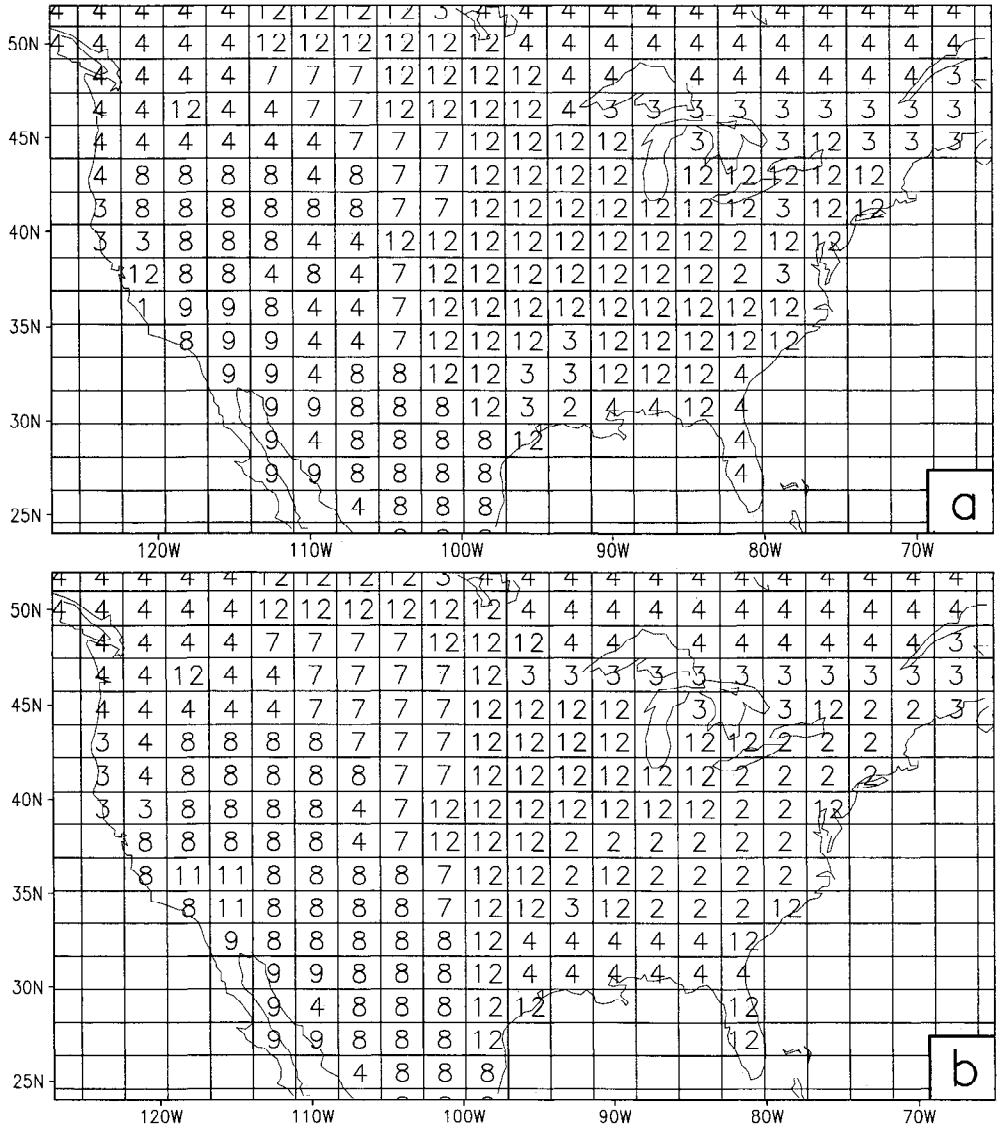

Figure 2. Vegetation types for (a) OLD simple biosphere model (SiB) vegetation map and (b) U.S. Geological Survey (USGS) SiB vegetation map. Types are the following: 2, broadleaf deciduous trees; 3, broadleaf and needleleaf trees; 4, needleleaf evergreen trees; 7, grassland; 8, broadleaf shrubs with perennial groundcover; 9, broadleaf shrubs with bare soil; 11, bare soil; 12, crops.

implied stronger than observed moisture transfer from the Gulf of Mexico, the simulated rainfall was 1 mm d^{-1} (30%) less than observed in the central United States (Figure 3b). This supports the idea that the main moisture source for central U.S. summer precipitation is land surface evaporation. The hydrological cycle will be discussed in more detail in section 4.

4. Impact of Vegetation on the Model Systematic Errors

4.1. Replacing Crops With Trees Impact

The preceding analysis led to the hypothesis that the use of the crop vegetation type (type 12) is related to the occurrence of model systematic errors over the central United States. For a grid box in the GCM covered by the crop vegetation type, 8% of the area is assumed to be covered by broadleaf deciduous trees. In the new SiB vegetation map the type 12 vegetation in the eastern part of the United States was replaced by type 2. A comparison of Figures 1a and 3a shows that the temperature bias in the eastern United States was reduced in the new map simulation. To test whether the remaining positive bias was related to the crop vegetation, we replaced the crops by trees over the entire United States. An ensemble of three integrations with the same three initial conditions and SST as used in ensemble C was done in which all the SiB vegetation type 12 points over the United States were replaced with type 2. These integrations will be referred to as T1, T2, and T3 (Table 1). The most important parameters of vegetation types 2 and 12 are listed in Table 2. The vegetation cover, leaf area index, and green leaf fraction of type 12 change with the crop growing season, which is the function of latitude and calendar day. For vegetation type 2 the leaf area index and green leaf fraction are a function of the month and are given for each month in Table 2.

Figure 5a shows the JJA mean surface air temperature difference between ensemble T (mean of T1, T2, and T3) and

Table 1. Initial and Boundary Conditions

Cases	Initial Conditions	SST Conditions	Land Surface Condition
C1	June 1, 1987	1987 SST	control
C2	June 1, 1988	1988 SST	control
C3	June 1, 1993	1993 SST	control
T1	June 1, 1987	1987 SST	as C1, but type 12 replaced by type 2
T2	June 1, 1988	1988 SST	same as T1
T3	June 1, 1993	1993 SST	same as T1
V1	June 1, 1987	1987 SST	as C1, but the vegetation canopy properties of type 12 replaced with those of type 2
V2	June 1, 1988	1988 SST	same as V1
V3	June 1, 1993	1993 SST	same as V1
S1	June 1, 1987	1987 SST	as C1, but the soil properties of type 12 replaced with those of type 2
S2	June 1, 1988	1988 SST	same as S1
S3	June 1, 1993	1993 SST	same as S2
A1	June 1, 1987	1987 SST	as C1, but the aerodynamic properties of type 12 replaced with those of type 2
A2	June 1, 1988	1988 SST	same as A1
A3	June 1, 1993	1993 SST	same as A1
ST	June 1, 1987	1987 SST	as C1, but stomatal resistances of type 12 replaced with those of type 2
SE1	June 1, 1987	1987 SST	crops specified by new seasonality
SE2	June 1, 1988	1988 SST	crops specified by new seasonality
SE3	June 1, 1993	1993 SST	crops specified by new seasonality

Different cases will be described in the text. SST, sea surface temperature.

ensemble C (mean of C1, C2, and C3). The large negative surface temperature difference (up to more than 3°K) is well situated to correct much of the model positive temperature bias shown in Figure 3a. The temperature bias in the lower atmosphere was also substantially reduced (not shown). This reduction occurred in all three cases and in all three months, with the greatest reduction occurring in the last 2 months. Among the three cases, case T2 (a dry year) had the largest impact, and case T3 (a wet year) had the smallest impact (not shown). The negative precipitation bias was also reduced in ensemble T relative to that in ensemble C (Figure 5b). The T-C precipitation differences displayed more month to month variability than the surface temperature differences. The JJA mean rainfall difference over the central United States was 0.5–1 mm d^{-1} (20–40% of the precipitation in ensemble C). There are relatively small differences in temperature and precipitation over the northwestern United States, where the vegetation properties were not changed. Such differences may be induced by circulation changes related to the central U.S. anomalies or may be the result of the internal variability in the GCM.

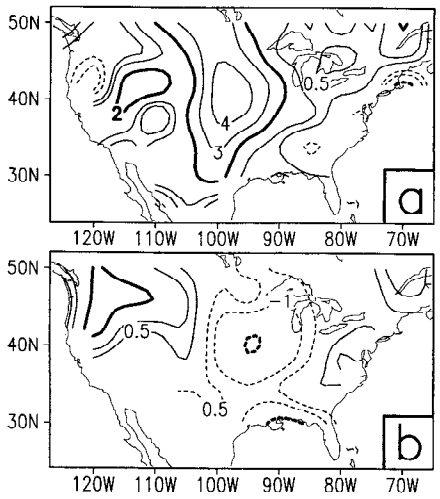

Figure 3. Ensemble C JJA systematic error in (a) surface temperature, contours are ±0.5°, 1°, 2°, 3°, 4°C, and (b) precipitation, contours are ±0.5, 1, 2 mm d^{-1}. Dashed contours are negative.

The JJA mean evaporation difference between ensemble T and ensemble C is shown in Figure 5c. The region of positive evaporation differences is coincident and consistent with the precipitation and surface temperature differences. Consistent with the cooler temperatures in the central United States, there was a reduction in the air flow from the Gulf of Mexico (Figure 5c) and vertically integrated moisture flux convergence (Figure 5d). However, the increased land surface evaporation in ensemble T was the dominant change in the moisture and surface energy balances, resulting in more precipitation and lower surface temperatures in ensemble T.

4.2. Impact of Different SSiB Parameter Sets

The above experiment demonstrates that the systematic errors in the surface temperature and precipitation fields are related to the SiB crop vegetation type. There are about 20 physiological, morphological, and physical parameters in SSiB. Experiments have been designed to determine which parameters of vegetation type 12 are related to the systematic errors. As the albedo is similar for crop and deciduous trees in SSiB, its impact will not be tested here. Because of the internal variability in the GCM, it is difficult to test the impact of each individual parameter. We tested four groups of parameters: vegetation canopy properties, soil properties, aerodynamic properties, and stomatal resistances. Vegetation canopy properties tested include vegetation cover, leaf area index, and green leaf fraction; soil properties tested include soil depth, hydraulic conductivity at saturation, soil water potential at saturation, and porosity; aerodynamic properties tested include surface roughness length, zero displacement height, vegetation height, and bulk aerodynamic resistance at the canopy air space.

In each experiment the values of one of these groups of crop parameters were replaced by the corresponding broadleaf deciduous tree parameters globally. The integrations are listed in Table 1. For each experiment we conducted three integrations with the same initial conditions and SST used in ensembles C

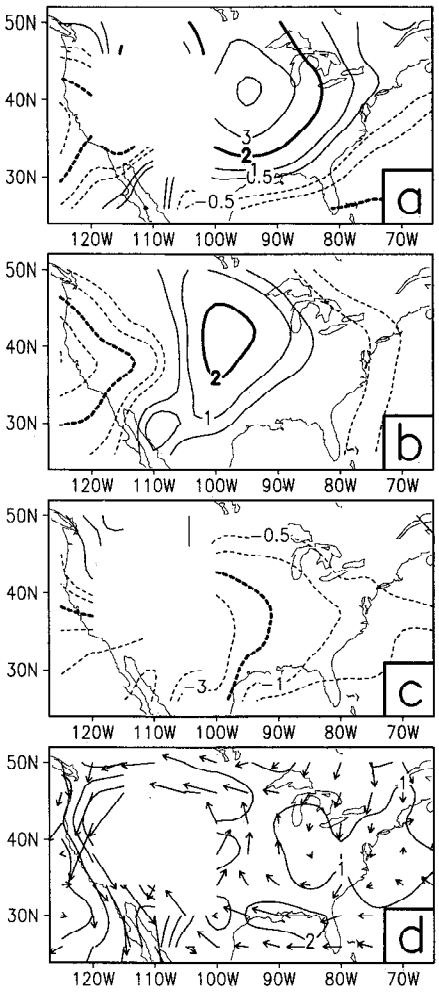

Figure 4. Ensemble C JJA systematic error in (a) 850-mbar temperature, (b) 700-mbar temperature, contours are ±0.5°, 1°, 2°, 3°, 4°C, (c) 850-mbar specific humidity, contours are ±0.5°, 1°, 2°, 3°, 4°, 6° g kg^{-1}, and (d) 850-mbar wind, isotachs are 1, 2, 3 m s^{-1}. Dashed contours are negative.

and T. We will refer the ensemble means as ensembles V, S, A, and ST for vegetation canopy properties, soil properties, aerodynamic properties, and stomatal resistance, respectively. The minimum stomatal resistance for crops and broadleaf deciduous trees are the same (Table 2). Thus we only tested the stress factors in the stomatal resistance experiment, and no substantial impact was found (not shown). Therefore we will focus on the results from the other three experiments.

Table 2. Vegetation and Soil Properties for Type 2 and Type 12

	Type 2	Type 12
Vegetation cover	0.75	0–0.9
Leaf area index (J,J,A)	5.08, 5.38, 4.88	0–6
Green leaf fraction (J,J,A)	0.93, 0.83, 0.70	0–0.9
Minimum stomatal resistance, s m^{-1}	209	209
Surface roughness, m	1.04	0.49
Displacement height, m	16.62	12.39
Depth of soil layers, m	0.02, 1.48, 2.00	0.02, 0.47, 1.00
Hydraulic conductivity of Saturated soil, m s^{-1}	0.2×10^{-4}	0.35×10^{-5}
Surface albedo	0.13	0.13

Figures 6a, 6b, and 6c show the JJA mean surface temperature differences between ensembles V, S, A and ensemble C, respectively. In each ensemble the surface temperature was reduced in the central United States where the parameter values were changed. The vegetation canopy properties had the largest impact on the surface temperature simulations. In ensemble T the surface temperature averaged over the region 30° to 45°N and 90° to 105°W was reduced by 2.2K° relative to that in ensemble C. We will refer to this area as the reference area, for which area-averaged JJA mean values are given in

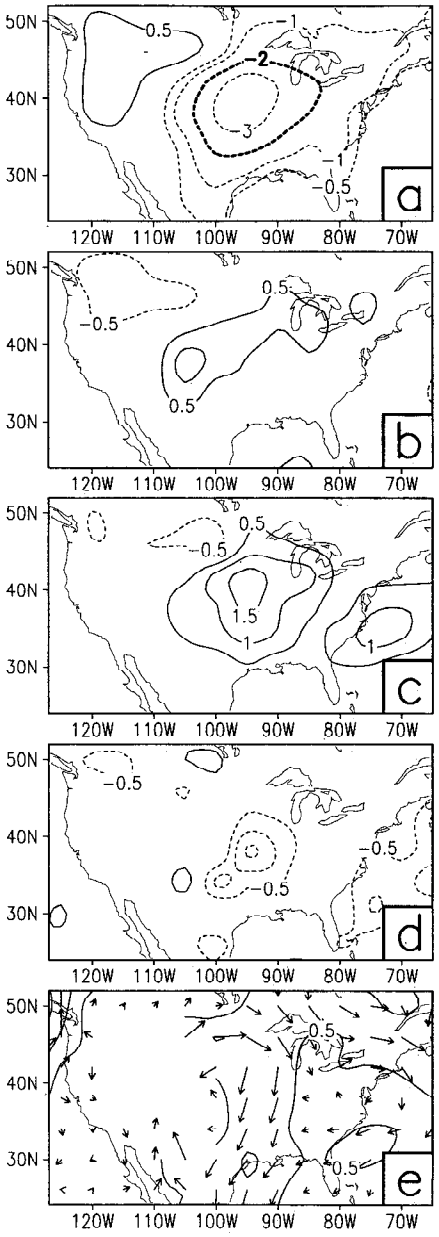

Figure 5. JJA mean ensemble T minus ensemble C difference in (a) surface air temperature, contours are ±0.5°, 1°, 2°, 3°C (b) precipitation, contours are ±0.5, 1 mm d^{-1}, (c) evaporation, contours are ± 0.5, 1, 1.5 mm d^{-1}, (d) vertically integrated moisture flux convergence, contours are ±0.5, 1, 1.5 mm d^{-1}, and (e) 850-mbar wind, isotachs are 0.5, 1 m s^{-1}. Dashed contours are negative.

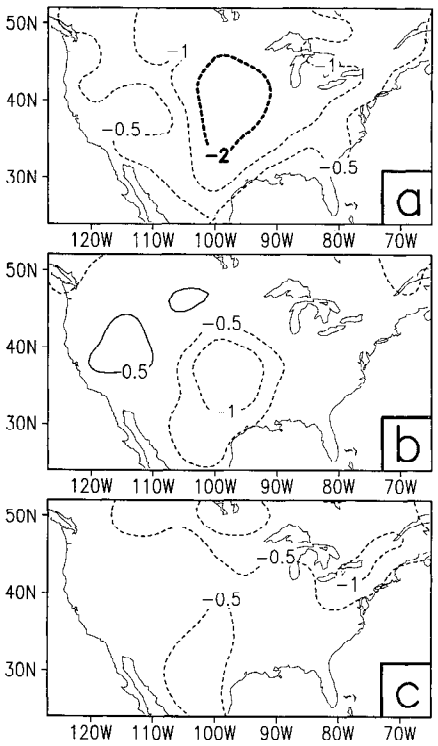

Figure 6. JJA mean difference in surface air temperature for (a) ensemble V minus ensemble C, (b) ensemble S minus ensemble C, and (c) ensemble A minus ensemble C. Contours are ±0.5°, 1°, 2°C. Dashed contours are negative.

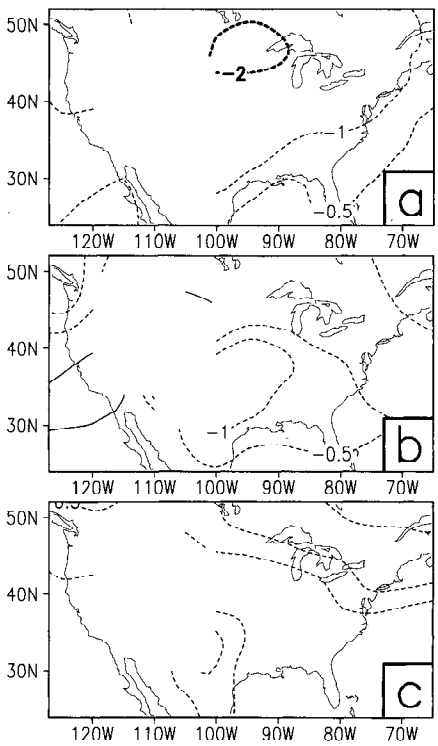

Figure 7. JJA mean difference in 850-mbar temperature for (a) ensemble V minus ensemble C, (b) ensemble S minus ensemble C, and (c) ensemble A minus ensemble C. Contours are ±0.5°, 1°, 2°C. Dashed contours are negative.

Table 3. Most of the grid boxes in this area were originally assigned vegetation type 12. In ensemble V there was a 1.8°K reduction relative to ensemble C, or 83% of the reduction in ensemble T. The soil properties had the second largest impact (ensemble S), reducing the surface temperature by 0.8°K, or 36% of the reduction in ensemble T. The aerodynamic properties had the least impact among the three groups, reducing the surface temperature by about 0.4°K, or 16% of the reduction in ensemble T. Because of nonlinearity, the sum of the three reductions in ensembles V, S, and A do not equal to the reduction in ensemble T. The impacts in the lower levels of the atmosphere are similar to those at the surface. The reference area temperatures were reduced by 1.7°K, 1.0°K, and 0.4°K at 850 mbar (Table 3 and Figure 7) and 0.9°K, 0.7°K, and 0.2°K at 700 mbar (not shown) for ensembles V, S, and A, respectively.

The temperature reductions were caused by changes in the surface energy budget. The energy budget at the surface averaged over the reference area is shown in Table 3. The changes in latent heat flux dominate the surface energy balance. Ensemble V had the largest latent heat flux increase, 25 W m^{-2} in the reference area. The latent heat flux was increased by 14 and 8 W m^{-2} in ensembles S and A. The surface evaporation differences for ensemble V, S, and A are shown in Figures 8a–8c, respectively. The latent heat flux increase in ensemble V was mainly due to increased direct evaporation of moisture intercepted by the canopy. In ensemble S the increase in latent heat was caused by increased evaporation from the bare soil, which was enhanced by the higher hydraulic conductivity of the vegetation type 2 soil. Vegetation type 2 also has deeper soil layers, which yields more available soil water (Table 2). Sensible heat flux changes were smaller and of opposite sign of the latent heat flux changes. Cloud cover was increased in all the ensembles (not shown) and less short wave radiation reached the ground. The downward long wave radiation reaching the

Table 3. JJA Mean Energy Balance at the Surface

	Ensembles					
	C	T-C	V-C	S-C	A-C	SE-C
Surface temperature	24.7 (2.6)	−2.2 (85%)	−1.8 (82.9%)	−0.8 (35.5%)	−0.4 (16.6%)	−2.2 (85%)
Temperature at 850 mbar	20.1 (2.2)	−1.8 (82%)	−1.7 (77%)	−1.0 (45%)	−0.4 (18%)	−2.3 (104%)
Latent heat	73	26	25	14	8	37
Sensible heat	89	−15	−19	−10	−9	−31
Downward short wave radiation	268	−6	−9	−10	−4	−20
Downward long wave radiation	373	0	0	7	4	5
Upward long wave	479	−17	−15	−7	−1	−21

Averaged over latitude 30°–45°N and longitude 90°–105°W. The units are W m^{-2} for fluxes and degrees celsius for temperature. The number in parentheses are errors (for ensemble C) or relative differences from ensemble C errors (for other ensembles).

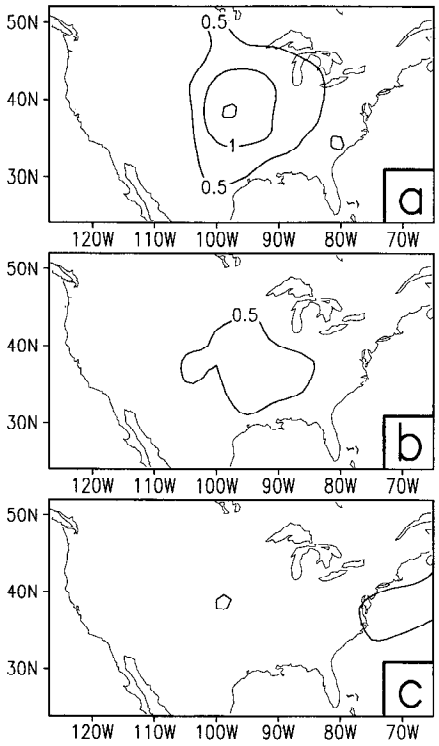

Figure 8. JJA mean difference in evaporation for (a) ensemble V minus ensemble C, (b) ensemble S minus ensemble C, and (c) ensemble A minus ensemble C. Contours are ±0.5, 1, 1.5 mm d^{-1}. Dashed contours are negative.

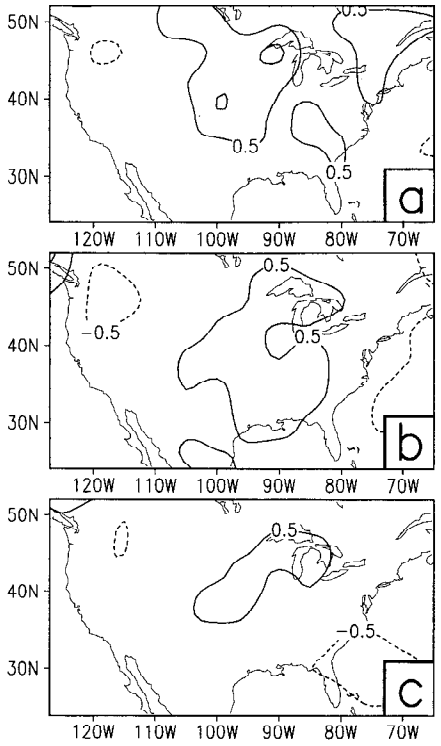

Figure 9. JJA mean difference in precipitation for (a) ensemble V minus ensemble C, (b) ensemble S minus ensemble C, and (c) ensemble A minus ensemble C. Contours are ±0.5, 1, 1.5 mm d^{-1}. Dashed contours are negative.

ground tended to increase in the experiments due to the higher cloud cover and moister atmosphere. However, the downward long wave radiation changes were small in magnitude. To maintain the energy balance, the upward long wave radiation and surface temperature were reduced, consistent with the increased latent heat flux. Ensemble V had the largest changes in the surface evaporation and the surface temperature among ensembles V, A, and S.

Several components of the JJA mean water cycle averaged over the reference area are shown in Table 4. The precipitation increases were similar in experiments V, S, and A, with increases of 0.4–0.5 mm d^{-1} over the reference area in each experiment (Figure 9 and Table 4). Surface evaporation and moisture flux convergence are the major moisture sources for the water cycle. In these experiments, surface evaporation changes dominated the water budget. Although ensemble V had the largest evaporation increase, it also had reduced moisture flux convergence. The 850-mbar specific humidity in the reference area increased by 0.8 g kg^{-1} in ensemble V, which is less than the increase in ensemble S (1.2 g kg^{-1}). Ensemble S had a modest evaporation increase, but the moisture flux convergence was slightly increased. Ensemble A had the smallest increase in evaporation, but higher surface roughness led to an increase in moisture flux convergence, as found by Sud et al. (1988).

Table 4. JJA Mean Water Cycle Components

	Ensembles					
	C	T-C	V-C	S-C	A-C	SE-C
Precipitation	2.69 (−0.93)	0.45 (48%)	0.46 (49%)	0.47 (50%)	0.34 (37%)	0.8 (86%)
Evaporation	2.5	0.9	0.9	0.5	0.3	1.3
Integrated moisture flux convergence	−0.7	−0.4	−0.2	0.2	0.2	−0.3
Specific humidity at 850 mbar	10.3 (−1.9)	0.9 (47%)	0.8 (42%)	1.2 (63%)	0.4 (21%)	1.7 (89%)

Averaged over latitude 30°–45°N and longitude 90°–105°W. The units for specific humidity are g kg^{-1}. The units for other variables are mm d^{-1}. The number in parentheses are the errors (for ensemble C), or relative differences from ensemble C errors (for other ensembles).

5. Impact of Vegetation Seasonality

The preceding analysis reveals that the dominant parameters responsible for the systematic bias related to the crop vegetation type are the vegetation canopy properties: vegetation cover, leaf area index, and green leaf fraction. In SiB these parameters are determined by the crops' growing stage, which is a function of latitude and calendar date. Empirical equations based on the crop growing conditions in Europe are used to describe the seasonality of the vegetation cover, leaf area index, and green leaf fraction of crops [*Sellers and Dorman*, 1987]. Although these equations are based on field measurements, the application of these equations to large spatial scales is problematic. For example, the harvest only requires a few days, resulting in a sharp transition in the crop parameters in time. Even in one GCM grid box (about 200 km on a side), the variations of the harvest date could easily be more than a couple of days. For grid boxes at the same latitude but at widely different longitudes, the differences in harvest date could be much larger. The crop model assumes that the leaf

area index and some other vegetation properties are equal to zero after harvest. Thus it makes the agricultural areas almost equivalent to a desert after the harvest.

The June 1 to August 30 daily time series of simulated surface temperature (solid line), the observed surface temperature (starred line, from monthly data) and the simulated leaf area index (boxed line) for the southern (32°–37°N), middle (37°–42°N), and northern (42°–47°N) belts of the 89°–100°W crop region are shown in Figures 10a–10c, respectively. The simulated surface temperature is the equivalent radiative temperature from the previously discussed 30 case ensemble. During the ripening, harvest, and cutting stages the leaf area index radip drops to zero. Coincidentally, the positive surface temperature biases develop. After the leaf area index reached zero the surface temperature biases persist. This relation is also reflected in Figure 1. The positive surface temperature bias in June occurred only in the southern United States (Figure 1b), where the harvest was already in progress. The positive temperature bias was fully developed over the entire agricultural area in July, when the harvest was in progress or completed over the entire region (Figure 1c).

The drastic reduction shown in the leaf area index also occurs in the simulated vegetation cover and greenleaf fraction. Such dramatic reductions are not supported by satellite observations over large areas. Recently published satellite data included on the ISLSCP CD ROM [*DeFries and Townshend*, 1994; *Sellers et al.*, 1995] show that during the boreal summer period the NDVI, leaf area index and green leaf fraction remained stable. On the basis of the above analysis of model results and the ISLSCP observational data, we have modified the seasonality of the leaf area index, green leaf fraction, and vegetation cover to be more realistic for average crop conditions over large areas.

Figure 11 shows the leaf area index for the old crop model and the new crop model for 40°N. In the old model, the leaf area index drastically reduces to zero after the harvest. In the new model, we retain the old leaf area index in the emergence and jointing stages since we have not found biases in the GCM simulations during these two stages and the seasonality of the leaf area index is consistent with that from the ISLSCP CD ROM. The seasonal variations of the leaf area index in other months have been altered to follow that from the ISLSCP CD ROM.

Because our results indicate that the crop soil properties also contribute to the systematic bias, we also replace the soil parameters of crops with those of broadleaf deciduous trees, which cover much of eastern United States. Therefore, in the revised data set the soil properties are more uniform over a large region of the U.S., which is in agreement with the Zobler soil property map [*Zobler et al.*, 1986]. A recent study has shown considerable heterogeneity in the distribution of soil types across the contiguous United States [*Kern*, 1994]. Further research is required to determine the most appropriate soil data for use in GCM simulations. The aerodynamical parameters of crops are not changed as there is no physical basis to adapt trees' aerodynamic properties for use with crops.

Using the new seasonality and new soil properties data set, we integrated the model using the same three initial atmospheric conditions and SST boundary conditions as used in the previous experiments (Table 1). We refer the ensemble mean of these new integrations as ensemble SE. Figures 12a–12e show the JJA mean ensemble SE minus ensemble C difference in surface temperature, precipitation, surface evaporation, vertically integrated moisture flux convergence, and 850-mbar wind vectors, respectively. Comparing Figure 12 with Figures 3 and 4 and examining the results in Tables 3 and 4 reveals that much of the systematic error has been corrected. The positive temperature biases over the reference area in ensemble C were 2.6°K, 0.5°K, 4.0°K, and 3.5°K for JJA, June, July, August, respectively. In ensemble SE the corresponding systematic temperature biases are 0.4°, −0.6°, 0.9°, and 1.3°K. The major biases in July and August were reduced substantially. The improvements in the precipitation and specific humidity at 850 mbar in ensemble SE are even larger than those obtained in ensemble T. The precipitation biases over the reference area in ensemble C were −0.9, −0.8, −1.0, and −1.0 mm d^{-1} for JJA, June, July, and August. The corresponding rainfall biases in ensemble SE were −0.1, 0.1, −0.3, and −0.1 mm d^{-1}. The relative bias is reduced from 30% in ensemble C to 3% in ensemble SE.

This analysis has focused on the United States; however, there are four large crop areas in our global vegetation map. The other three are located in Europe, China, and India. The simulation in these areas are also improved (not shown).

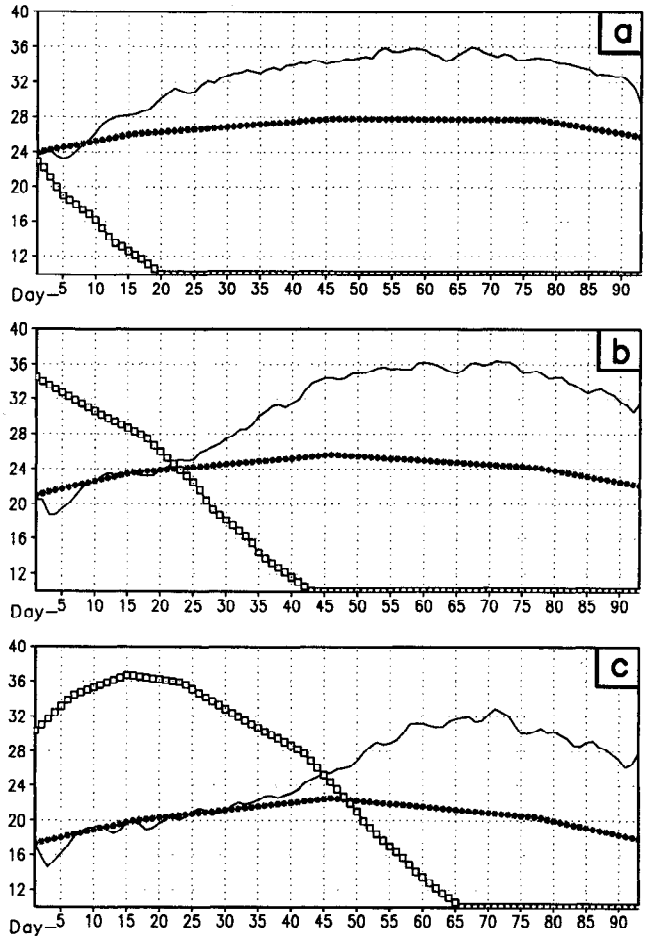

Figure 10. June 1 to August 30 daily time series of GCM surface temperature (degrees celsius, old 30 case ensemble, solid line), observed surface air temperature (degrees celsius, from monthly data, starred line), and simulated leaf area index (range from 0 to 6, boxed line) area averaged for 89°–100°W and (a) 32°–37°N, (b) 37°–42°N and (c) 42°–47°N.

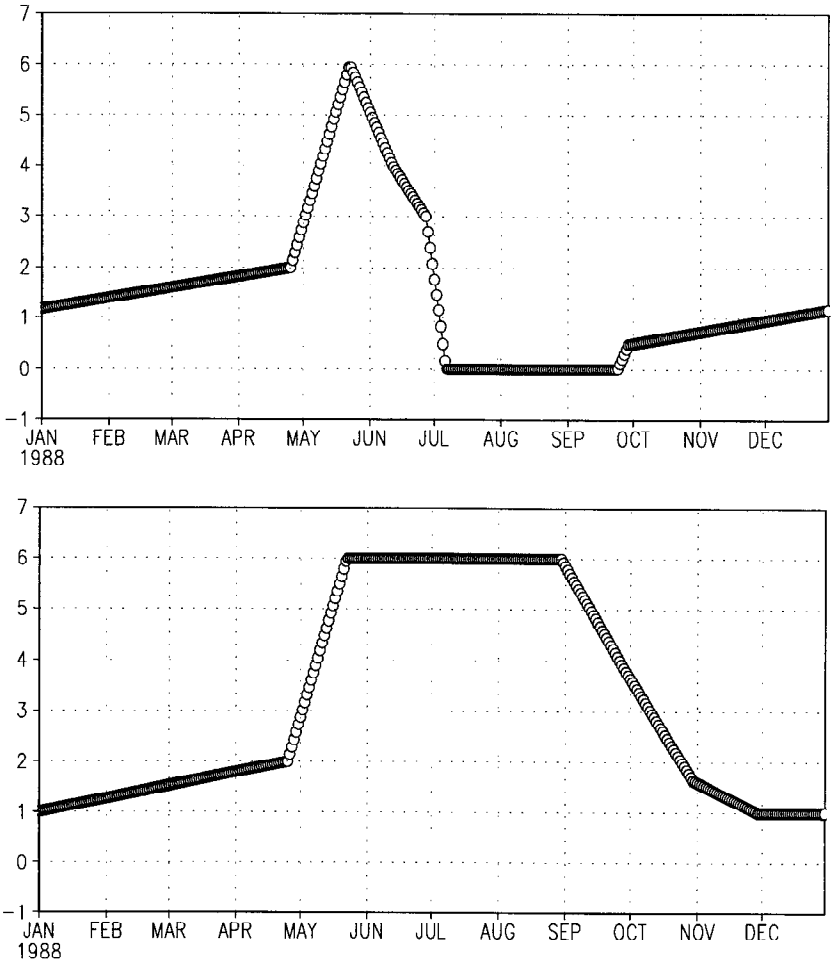

Figure 11. Annual cycle of crop leaf area index at 40°N: (a) old crop model; (b) new crop model.

6. Discussions and Conclusions

In this paper, systematic positive surface temperature biases and negative precipitation biases over the central United States during summer have been identified and analyzed. These systematic errors started to develop in June and became very significant during July and August. Experiments revealed that these errors were related to the SiB crop vegetation type in this region. The vegetation and soil properties of the crop vegetation type were divided into several groups, and the impact of each group on the systematic biases was tested in GCM experiments. The results show that the systematic errors were largely caused by the prescription of the vegetation seasonality in the crop model. The soil properties also contributed to these problems. On the basis of these results, the crop model has been improved and the systematic biases have been reduced.

In this study the surface evaporation was found to be the main moisture source over the central United States during summer. The JJA mean evaporation was 2.5 mm d^{-1} and integrated moisture flux convergence was -0.7 mm d^{-1} over the central U.S. reference area in the control integration ensemble. Moreover, in most of the anomaly experiments the changes in surface evaporation were much larger than the changes in moisture flux convergence. However, this is not always the case when the land surface conditions change. When the crop area over the southeastern United States in the old SiB map (Figure 2a) was replaced by the trees in the USGS SiB map (Figure 2b), the surface evaporation over the southeastern United States was slightly enhanced, but the integrated moisture flux convergence was reduced [*Fennessy and Xue*, 1995]. Because this area is very close to the ocean and the water vapor flux from the ocean is a major moisture source, the magnitude of the changes in moisture flux convergence was comparable to that of the surface evaporation, and the rainfall over the southeastern United States was not changed. Thus the mechanisms of land surface-atmosphere interactions depend on the geographical location.

In addition to improving the model in this study, valuable insights have been gained into the relative importance of different land surface properties for prediction. Among land surface properties, the effects of surface albedo, soil moisture and, to some extent, surface roughness have been widely examined in previous studies, because these parameters are explicitly specified in conventional GCMs. This study demonstrates that for U.S. summer monthly and seasonal predictions the vegetation seasonality also plays a crucial role. The results presented here have two implications for the use of a biosphere model in a GCM. First, biosphere models need more information about the land surface conditions, for example, a correct prescription of the vegetation properties and their geographical and temporal distribution. Second, coupled atmosphere-biosphere models may provide insights into the real-world interactions between different vegetation and soil properties and

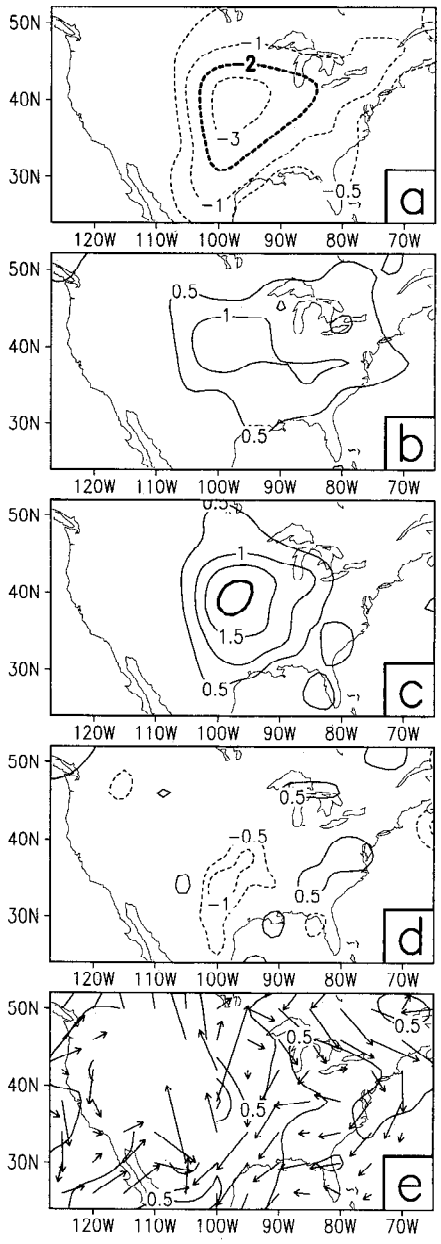

Figure 12. JJA mean ensemble SE minus ensemble C difference in (a) surface air temperature, contours are ±0.5°, 1°, 2°, 3°C (b) precipitation, contours are ±0.5, 1 mm d^{-1}, (c) evaporation, contours are ±0.5, 1, 1.5, 2 mm d^{-1}, (d) vertically integrated moisture flux convergence, contours are ±0.5, 1 mm d^{-1} and (e) 850-mbar wind, isotachs are 0.5, 1, 1.5 m s^{-1}. Dashed contours are negative.

the atmosphere. As more data are derived from satellite observations [*Meeson et al.*, 1995; *Sellers et al.*, 1995], we are optimistic that a more realistic description of the land surface conditions will became available.

There are 12 vegetation types in SSiB. The parameters for all but the crop vegetation type are currently prescribed in SSiB based on monthly climatological data. The growing stages for these types are not simulated by the model. It is ironic that a seemingly more realistic approach used for the crop model caused more problems because it requires more realistic data, which has not been available. While some detailed vegetation information may be important for micrometeorological processes, it may not be so critical for long-term and large-scale predictions. The scaling issue has to be taken into account. The new crop parameters developed in this study are based on the ISLSCP CD ROM. We did not use the ISLSCP data directly but rather adopted its annual cycle.

The first part of this study has shown that the specification of the vegetation distribution has a significant impact on the monthly and seasonal simulations of evaporation, surface air temperature, and precipitation over the United States in the COLA GCM. The second part of this study reveal that the vegetation parameter specification also has a strong impact on the seasonal simulations. The atmospheric response was largely limited to the regions where the land surface conditions were changed. We used three very different cases in this study, including an extremely dry year (1988) and an extremely wet year (1993). Yet the anomaly patterns caused by the land surface forcing were similar in all three cases. The magnitude of the impact was largest in the dry year (1988) and least in the wet year (1993). The interaction mechanisms between the land surface and the atmosphere are similar to those previously found for the tropics. This study demonstrates that even in the middle latitudes, monthly and seasonal predictability can be enhanced by correct specification of the land surface conditions.

Acknowledgments. The authors would like to thank J. Shukla and L. Steyaert for supporting this project, and also thank James McManus for providing the ISLSCP data. We would also like to thank E. Kalngy, K. Klink, K. Mitchell, and H.-L. Pan for very helpful discussions. This work was conducted under support from the National Oceanic and Atmospheric Administration (NOAA) through NOAA grant NA46GP0340-02 and the National Science Foundation (NSF), the Aeronautics and Space Administration (NASA) through NSF grants ATM-93-41271, ATM-93-21354, and EAR-94-05431. Computational support was provided by the NASA Center for Computational Sciences and NCAR Scientific Computing Division.

References

Alpert, J. C., M. Kanamitsu, P. M. Caplan, J. G. Sela, H. H. White, and E. Kalnay, Mountain induced gravity wave drag parameterization in the NMC medium-range forecast model, in *Proceedings of Eight Conference on Numerical Weather Prediction*, pp. 726–733, Am. Meteorol. Soc., Boston, Mass., 1988.

Anthes, R. A., A cumulus parameterization scheme utilizing a one-dimensional cloud model, *Mon. Weather Rev.*, *105*, 270–300, 1977.

Bonan, G. B., Comparison of the land surface climatology of the National Center for Atmosphere Research community climate model 2 at R15 and T42 resolution, *J. Geophys. Res.*, *99*, 10357–10364, 1994.

Chen F., K. Mitchell, J. Schaake, Y. Xue, H.-l. Pan, V. Koren, Q. Duan, and A. Betts, Modeling of land surface evaporation by four schemes and comparison with FIFE observations, *J. Geophys. Res.*, this issue.

Davies, R., Documentation of the solar radiation parameterization in the GLAS climate model, *NASA Tech. Memo*, *83961*, 57, 1982.

DeFries, R. S., and J. Townshend, NDVI-derived land cover classifications at a global scale, *Int. J. Remote Sens.*, *15*, 3567–3586, 1994.

Dorman, J. L., and P. Sellers, A global climatology of albedo, roughness length and stomatal resistance for atmospheric general circulation models as represented by the Simple Biosphere Model (SiB), *J. Appl. Meteorol.*, *28*, 833–855, 1989.

Fennessy, M., and Y. Xue, Impact of USGS vegetation map on GCM simulations over the United States, *Ecol. Appl.*, in press, 1995.

Fennessy, M. J., et al., The simulation Indian monsoon: A GCM sensitivity study, *J. Clim.*, *7*, 33–43, 1994.

Harshvardhan, R. Davies, D. A. Randall, and T. G. Corsetti, A fast radiation parameterization for general circulation models, *J. Geophys. Res.*, *92*, 1009–1016, 1987.

Hou, Y.-T., Cloud-radiation-dynamics interaction, Ph.D. dissertation, 209 pp., Univ. of Md., College Park, 1990.

Kern, J. S., Spatial patterns of soil organic carbon in the contiguous United States, *Soil Sci. Soc. Am. J.*, *58*, 439–455, 1994.

Kinter III, J. L., J. Shukla, L. Marx, and E. K. Schneider, A simulation of the winter and summer circulations with the NMC global spectral model, *J. Atmos. Sci.*, *45*, 2486–2522, 1988.

Klink, K., and C. J. Willmott, Notes on a global vegetation data set for use in GCMs, Dep. of Geogr., Univ. of Del., Newark, 1985.

Kuchler, A. W., World map of natural vegetation, in *Goode's World Atlas*, 16th ed., pp. 16–17, Rand McNally, Skokie, Ill., 1983.

Kuo, H. L., On formation and intensification of tropical cyclones through latent heat release by cumulus convection, *J. Atmos. Sci.*, *22*, 40–63, 1965.

Lacis, A. A., and J. E. Hanson, A parameterization for the absorption of solar radiation in the Earth's atmosphere, *J. Atmos. Sci.*, *32*, 118–133, 1974.

Loveland, T. R., J. W. Merchant, D. O. Ohlen, and J. F. Brown, Development of a land-cover characteristics database for the conterminous U.S., *Photogramm. Eng. Remote Sens.*, *57*, 1453–1463, 1991.

Matthews, E., Prescription of land-surface boundary conditions in GISS GCM II: A simple method based on high-resolution vegetation data bases, *NASA Tech. Memo. 86096*, 20 pp., 1984.

Matthews, E., Atlas of archived vegetation, land-use and seasonal albedo data sets, *NASA Tech. Memo.*, *86199*, 53 pp., 1985.

Meeson, B. W., F. E. Coprew, J. M. P. McManus, D. M. Myers, J. W. Closs, K.-J. Sunday, and P. J. Sellers, *ISLSCP Initiative I-Global Data Sets for Land-Atmosphere Models, 1987–1988*, CD-ROM, vols. 1–5, USA-NASA-GDAAC-ISLSCP-001-USA-NASA-GDAAC-ISLSCP-005, NASA, Washington, D.C., 1995.

Mellor, G. L., and T. Yamada, Development of a turbulence closure model for geophysical fluid problems, *Rev. Geophys.*, *20*, 851–875, 1982.

Reed, B. C., T. R. Loveland, L. T. Steyaert, J. F. Brown, J. W. Merchant, and D. O. Ohlen, Designing global land cover databases to maximize utility, in *Environmental Information Management and Analysis: Ecosystem to Global Scales*, edited by W. K. Michener, J. W. Brunt, and S. G. Stafford, pp. 299–314, Francis and Taylor, London, 1994.

Ropelewski, C. F., J. E. Janowiak, and M. F. Halpert, The analysis and display of real time surface climate data, *Mon. Weather Rev.*, *113*, 1101–1107, 1985.

Rowell, D., and C. Blondin, The influence of soil wetness distribution on short-range rainfall forecasting in the West African Sahel, *Q. J. R. Meteorol. Soc.*, *116*, 1471–1485, 1990.

Sato, N., P. J. Sellers, D. A. Randall, E. K. Schneider, J. Shukla, J. L. Kinter III, Y.-T. Hou, and E. Albertazzi, Effects of implementing the simple biosphere model in a general circulation model, *J. Atmos. Sci.*, *46*, 2757–2782, 1989.

Sela, J. G., Spectral modeling at the National Meteorological Center, *Mon. Weather Rev.*, *108*, 1279–1292, 1980.

Sellers, P. J., and J. L. Dorman, Testing the Simple Biosphere model (SiB) using point micrometeorological and biophysical data, *J. Appl. Meteorol.*, *26*, 622–651, 1987.

Sellers, P. J., Y. Mintz, Y. C. Sud, and A. Dalcher, A simple biosphere model (SIB) for use within general circulation models, *J. Atmos. Sci.*, *43*, 505–531, 1986.

Sellers, P. J., W. J. Shuttleworth, J. L. Dorman, A. Dalcher, and J. M. Roberts, Calibrating the simple biosphere model for Amazonian tropical forest using field and remote sensing data, 1, Average calibration with field data, *J. Appl. Meteorol.*, *28*, 727–759, 1989.

Sellers, P. J., M. D. Heiser, and F. G. Gall, Relations between surface conductance and spectral vegetation indices as intermediate (100 m^2 to 15 km^2) length scale, *J. Geophys. Res.*, *97*, 19033–19060, 1992.

Sellers, P. J., et al., An overview of the ISLSCP initiative I global data sets, in *ISLSCP Initiative I-Global Data Sets for Land-Atmosphere Models, 1987–1988*, CD-ROM, vol. 1, USA-NASA-GDAAC-ISLSCP-001, overview.doc, NASA, Washington, D.C., 1995.

Shao, Y., and A. Henderson-Sellers, Soil moisture simulation workshop review, *Global Planet. Change*, in press, 1995.

Slingo, J. M., The development and verification of a cloud prediction scheme for the ECMWF model, *Q. J. R. Meteorol. Soc.*, *103*, 29–43, 1987.

Steyaert, L. T., T. R. Loveland, J. F. Brown, and B. C. Reed, Integration of environmental simulation models with satellite remote sensing and geographic information systems technologies: Case studies, in *Proceedings: Pecora 12 Symposium on Land Information from Space-Based Systems*, pp. 407–417, Am. Soc. of Photogramm. and Remote Sens., Bethesda, Md., 1994.

Sud, Y. C., J. Shukla, and Y. Mintz, Influence of land surface roughness on atmospheric circulation and rainfall: A sensitivity study with a general circulation model, *J. Appl. Meteorol.*, *27*, 1036–1054, 1988.

Tiedtke, M., The effect of penetrative cumulus convection on the large-scale flow in a general circulation model, *Beitr. Phys. Atmos.*, *57*, 216–239, 1984.

Willmott, C. J., and K. Klink, A representation of the terrestrial biosphere for use in global climate studies, in *ISLSCP, Proceedings of an international conference*, pp. 109–112, Eur. Space Agency, Paris, 1986.

Xue, Y., and J. Shukla, The influence of land surface properties on Sahel climate, I, desertification, *J. Clim.*, *6*, 2232–2245, 1993.

Xue, Y., P. J. Sellers, J. L. Kinter III, and J. Shukla, A simplified biosphere model for global climate studies, *J. Clim.*, *4*, 345–364, 1991.

Xue, Y., N. Bastable, P. Dirmeyer, and P. Sellers, Sensitivity of simulated surface fluxes to changes in land surface parameterization—A study using ABRACOS data, *J. Appl. Meteorol.*, this press, 1995a.

Xue, Y., F. J. Zeng, and C. A. Adam, SSiB and its sensitivity to soil properties—A case study using HAPEX-Mobilly data, *Global Planet. Change*, this press, 1995b.

Zobler, L., A world soil file for global climate modeling, *NASA Tech. Memo.*, *87802*, 1986.

M. J. Fennessy and Y. Xue, Center for Ocean-Land-Atmosphere Studies, Calverton, MD 20705.

P. J. Sellers, NASA Goddard Space Flight Center, Code 923, Greenbelt, MD 20771.

(Received February 8, 1995; revised June 1, 1995;
accepted June 21, 1995.)